Introduction

Conventional migration tools have been implemented by the application of adjoint operators. Under simple circumstances this approach provides satisfactory results. In situations where the overburden is complex, scattering from the target is not simple, the acquisition geometry is irregular, or the waveforms are not spectrally balanced, adjoint operators often do not provide images of sufficient quality. These may be manifested as artifacts in the image, poor resolution, acquisition footprint or incomplete signature removal. In principle, we can use inversion to correct for these effects. Doing so can lead to images that are higher resolution, artifact-reduced, properly amplitude balanced and with a broadband spectrum (Wang et al., 2012).

Least-Squares Migration (LSM) is an improved approximation of the inverse operator (Schuster, 1993; Nemeth et al., 1999; Tang, 2008; Kaplan et al., 2010; Dai et al., 2011; Gang et al., 2012). The LSM has been implemented in either model space domain (Tang, 2008; Aoki et al., 2009; Dai et al., 2011) or time domain (Tang et al., 2009; Dai et al., 2010; Zhan et al., 2010). In our study, we chose the time domain LSM approach and used RTM as the engine for the forward modeling and migration.

Least-Squares Reverse Time Migration (LSRTM) can effectively suppress conventional migration artifacts including migration swings, side lobes and the acquisition footprint. There are, however, still some fundamental issues which need to be addressed for the practical implementation. These include the limits of our knowledge and the available options of the physics we use in forward modeling operators. We are also limited by the distortion caused by incomplete illumination, complex scattering, and spectral distortions that are observed in difficult imaging situations (Wang et al., 2012). All these issues impede the practical implementation of LSRTM. In this paper, we will share some lessons learned for LSRTM from our study.

Theory and Implementation

The least-squares migration can be represented by the following equation:

$$m_{mig} = (L^T L)^{-1} L^T d_{obs} \tag{1}$$

where, m_{mig} is the migration image, L represents the forward modeling operator, and d_{obs} is the observed seismic data. An iterative solution can be obtained by minimizing the objective function $p(m)$, which is the misfit between the forward modeled data Lm and the seismic data d_{obs}:

$$p(m) = \| Lm - d_{obs} \| \tag{2}$$

However, for practical implementation, the misfit calculation is not trivial due to the fact that the wave propagation through the real earth is far more complicated than an acoustic wave equation can describe. For example, the visco-elastic property of the earth cannot be simulated by our synthetic data generator. In turn, several modes, such as converted waves will be absent from the synthetic modeled data. These un-modelable modes in field data need to be removed through some prior preprocessing when we calculate the data misfit.

At the same time, the amplitude of the synthetic data is dependent upon the user defined source strength, and the wave propagator employed for modeling unavoidably introduces errors, especially amplitude errors. These issues prevent the synthetic data from matching the real data for long wavelengths. However, for the LSRTM approach the amplitudes are different at the wavelet level, and only these differences should be used to tune up the images. Thus proper scaling of the synthetic data is needed for the misfit calculation.

On the other hand, the artifacts caused by velocity errors are unavoidable in practice. For LSRTM, the migration and forward modeling are adjoint procedures, and the kinematic errors are usually minor for near offsets. But for far offsets, and especially for complex structure, velocity errors could cause events to be poorly aligned between the synthetic and observed data. This is similar to the cycle-skipping problem commonly observed in Full Waveform Inversion (FWI), which could cause the

inversion process divergence. To overcome this problem, we applied a proper matching filter on the synthetic data, which can effectively mitigate the poor alignment effects caused by velocity errors. Thus, for practical implementation, we revised the objective function to be:

$$p(m) = \| p_m(Lm) - p_f d_{obs} \| \quad (3)$$

where, p_m indicates the preprocessing of and proper scaling and filtering of the synthetic data to match the observed field data, and p_f is the preprocessing for the observed field data.

The corresponding iterative solution is:

$$m^{k+1} = m^k - \alpha L^T [p_m(Lm^k) - p_f d_{obs}] \quad (4)$$

where, α is the optimized step length and k is number of iterations. This equation is an iterative approach for LSRTM in the data domain. It is actually a process that repeatedly projects the difference between the modeled data and the input data to the model domain. In our implementation, the Born modeling algorithm was used to generate modeled data from the image. From the equations, we can see the algorithm of the LSRTM procedure is very similar to full waveform inversion (FWI). Both of them are inversion-based algorithm. For both their target is to minimize the difference between the modeled data and the observed data. However, there are some differences between LSRTM and FWI. Firstly, their objectives are different. The objective for FWI is to derive a high resolution velocity model. LSRTM, is used to derive a better reflectivity image, so for LSRTM, a fixed background velocity model is used, and this makes it a linear inversion approach. This allows LSRTM to have a better convergence feature than FWI. Compared to FWI, The forward modeling for LSRTM is based on seismic reflectivity, which is indeed a demigration process. This makes LSRTM less sensitive to velocity errors than FWI.

Synthetic data example

We applied the LSRTM algorithm to the 2D Marmousi synthetic data. The reflectivity model is shown in Figure 1A. A marine streamer acquisition is simulated for the synthetic data recording.

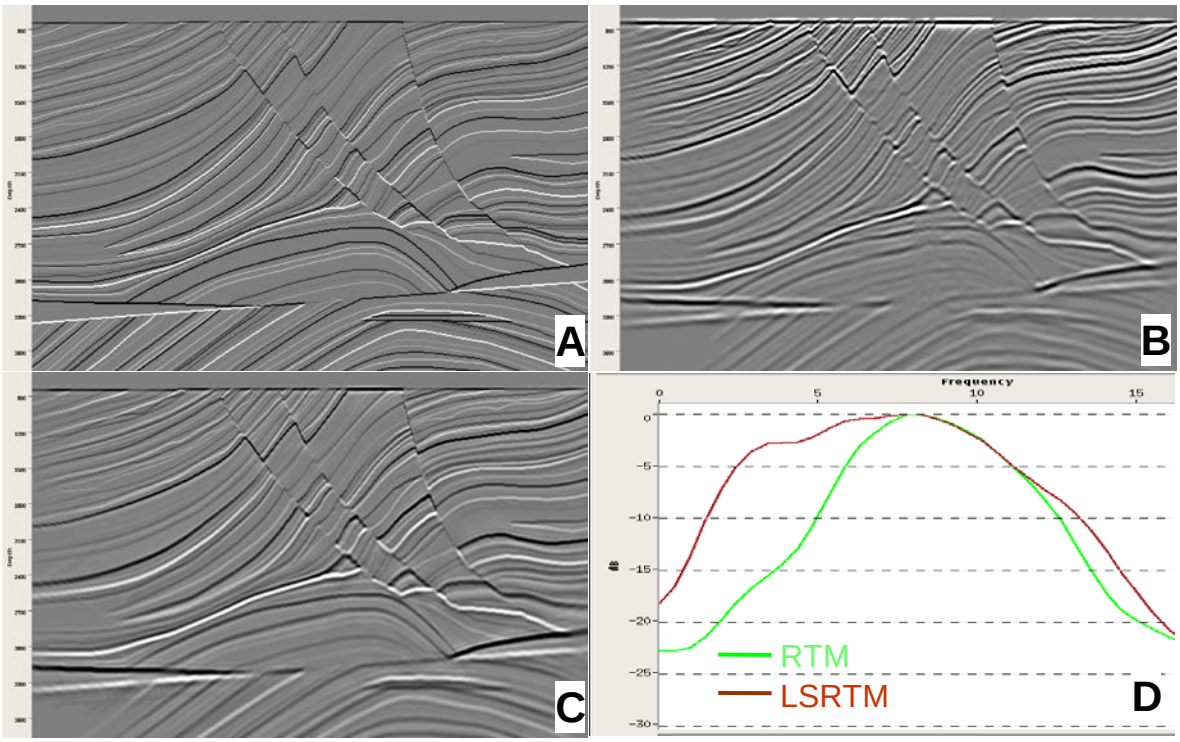

Figure 1. *(A) Marmousi reflectivity model. (B) Conventional RTM image of Marmousi synthetic data. (C) LSRTM image after 20 iterations. (D) Depth frequency spectrum comparison between conventional RTM and LSRTM images.*

The synthetic data set is generated with the finite difference solution of the acoustic wave equation with a 20 Hz Ricker source wavelet. Figure 1B shows the conventional RTM image, and Figure 1C shows the LSRTM image after the 20th iteration. Higher resolution is easily observed from the LSRTM image compared to the conventional RTM. Comparisons of the depth frequency spectra between the conventional RTM and LSRTM images are shown in Figure 1D. A broader frequency spectrum band in the LSRTM image is also apparent, since it recovered more energy especially on the low frequency end. The broadband image has a 3D textured appearance and higher lateral resolution. LSRTM can obtain broadband images through its iterative approach which gradually suppresses the side lobes of events in the seismic images. This approach is similar to deconvolution. The difference is that deconvolution suppresses the wavelet along only one direction, but LSRTM suppresses the side lobes in all 3D directions.

Field data examples

Both conventional RTM and LSRTM algorithms are applied to a 2D field data set from the Gulf of Mexico (GOM). Two groups of faults in two crossing directions are observed in this area. For the conventional RTM image (Figure 2A), some faults are not well-imaged and are poorly resolved. The LSRTM image (Figure 2B) shows improvements in the steep faults area, where the faults look more continuous. Some detailed features are beginning to appear. Weak energies, which are not properly migrated in conventional RTM are gradually recovered in LSRTM iterations. In overall appearance, we can also see a 3D textured looking effect from the LSRTM image, and the faults and layer boundaries look sharper and high resolution.

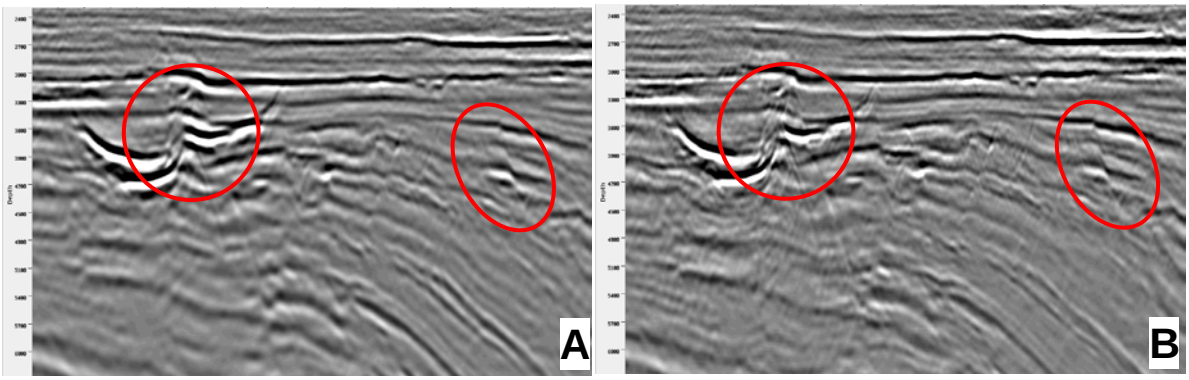

Figure 2 *The migration images of a data set from the GOM. (A) The conventional RTM image. (B) The LSRTM image after 5 iterations.*

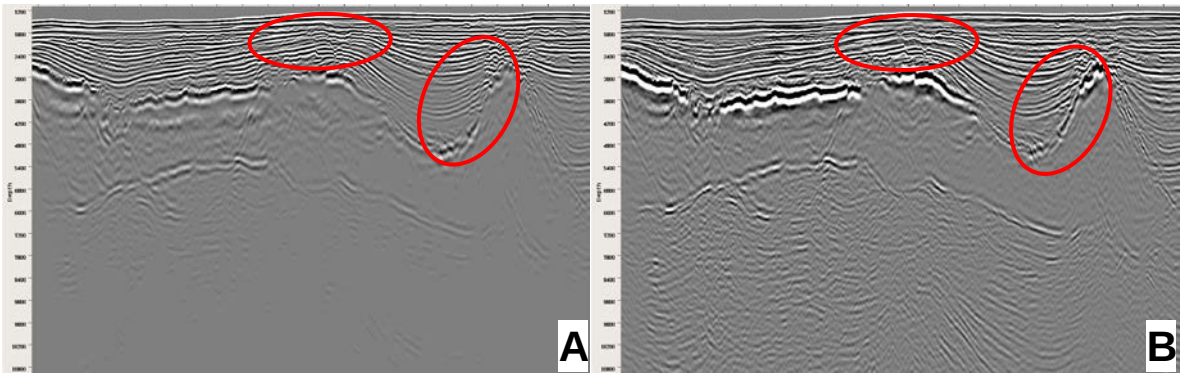

Figure 3 *The migration images of a data set from the GOM. (A) The Conventional RTM image. (B) The LSRTM image after 5 iterations.*

We also applied the LSRTM algorithm to a 3D field data set from the GOM. We can see some issues from the conventional RTM image (Figure 3A). Firstly, the image amplitude is not balanced. The sediments below salt look very weak. Secondly, the top of salt boundary contains some artifacts and looks smeared. For the LSRTM image (Figure 3B), the sediments below salt have more balanced

amplitudes. The reduction in artifacts in the LSRTM makes the top salt boundary better imaged. In shallow section, better fault definition and clearer event terminations near fault planes are observed. These improvements are attributable to the LSRTM's true amplitude feature.

Conclusions

We have implemented a time domain 3D LSRTM algorithm and applied it to both synthetic and field data examples. From the examples, LSRTM is demonstrated to be useful in providing close to true amplitude reflectivity images. The LSRTM is a 3D inversion based process and is a possible broadband imaging solution, conceptually like a 3D deconvolution. LSRTM can effectively broaden the low frequencies and suppress the side lobes, which gives the image a 3D textured effect, increases the resolution at sharp boundaries and improves steeply dipping events. It also improves lateral resolution such as fault definition. Because LSRTM is a true amplitude approach, it is an effective tool for 4D and for detailed reservoir imaging and interpretation.

Acknowledgements

We would like to thank the following TGS colleagues for their contributions and helpful discussions: Kwangjin Yoon, Jean Ji, Zhigang Zhang, and Zhiming Li, We also thank Laurie Geiger and Chuck Mason for reviewing and proof-reading this paper. Finally, we thank TGS management for permission to present this work.

References

Aoki, Naoshi, and Schuster, T., Gerard, 2009, Fast least-squares migration with a deblurring filter: Geophysics, **74**, 83-93.

Claerbout, J., 1992, Earth soundings analysis: Processing vs. inversion: Blackwell Scientific Publications, Inc.

Dai, Wei, Boonyasiriwat, C., and Schuster, T., Gerard, 2010, 3D Multi-source Least-squares Reverse Time Migration: SEG, Expanded Abstracts, **29**, 3120-3124.

Dai, Wei, Wang, Xin, Schuster, T., Gerard, 2011, Least-squares migration of multisource data with a deblurring filter: Geophysics, **76**, 135-146.

Gang Yao and Helmut Jakubowicz, 2012, Least-Squares Reverse-Time Migration. SEG, Expanded Abstracts, **30**, 1425-1429.

Kaplan, S.T., P.S. Routh, and M.D. Sacchi, 2010, Derivation of forward and adjoint operators for least-squares shot-profile split-step migration: Geophysics, **75**, s25-s35.

Nemeth, Tamas, Wu, Chengjun, and Schuster, T., Gerard, 1999, Least-squares migration of incomplete reflection data: Geophysics, **64**, 208-221.

Schuster, T., Gerard, 1993, Least-Squares Cross-Well Migration: SEG, Expanded Abstracts, **12**, 25-28.

Tang, Yaxun, 2008, Wave-equation Hessian by phase encoding: SEG, Expanded Abstracts, **27**, 2201-2205.

Tang, Yaxun, and Biodi, Biondo, 2009, Least-squares migration/inversion of blended data: SEG, Expanded Abstracts, **28**, 2859-2863.

Wang, B., Djikpesse, H., Etgen, J., Biondi, B., and Chávez-Pérez, S, 2012, Inversion-based High Resolution Imaging of Reservoirs., SEG Post-Convention Workshop.

Zhan, Ge, and Schuster, T., Gerard, 2010, Skeletonized Least Squares Wave Equation Migration: SEG, Expanded Abstracts, **29**, 3380-3384.